24th COBEM - 2017

24th ABCM International Congress of Mechanical Engineering
December 3-8, 2017, Curitiba, PR, Brazil

# COBEM-2017-2408
# DYNAMIC BEHAVIOR OF VISCOELASTIC ROTORS – A COMPARATIVE ANALYSIS

**Zoroastro F. Filho**
**Ubatan A. Miranda**
**Alex Álisson B. Santos**
SENAI CIMATEC - Orlando Gomes Avenue, 1845, Piatã, Salvador – Bahia-Brazil
zoro.fernandes@hotmail.com
ubatan.miranda@fieb.org.br
alex.santos@fieb.org.br

***Abstract.*** *Viscoelastic materials are widely used in industry and their modelling techniques are very useful for application in vibration damping problems linked with rotors and structural systems, contributing to the development of compact and efficient mechanical models. For the reduction of the rotors' weight, polymeric materials may be including in its construction. In view of this reality, the target of this paper is to present two theoretical numeric models to describe the dynamic behavior of viscoelastic rotors, evaluating and comparing their performances. From the Anelastic Displacement Fields (ADF) approach, introduced into the Lagrange equations by a differential operator in time domain, the equations of motion are getting by Rayleigh-Ritz approximation. Comparative analyses are performed for two different types of PVC and aluminum rotors, based on the results of the numerical resolution and theoretical references. The first model results in a good approximation for the aluminum, while the latter does for the PVC.*

***Keywords:*** *ADF, Viscoelasticity, Backward whirl, Hysteretic damping*

## 1. INTRODUCTION

Frequency dependent material properties, as loss factor and storage complex modulus are commonly reported in literature as damping properties in viscoelastic materials. Different time domain models representing viscoelastic linear behavior are possible, and many researchers, as assumed on this work, applies viscoelastic models in rotor dynamics considering small enough shaft strains in order to maintain this behavior.

Different viscoelastic models exist in literature relating stresses to strains, among others:

- Fractional Derivative (FD) – Proposed by Bagley and Torvik (1983) as the generalization of the standard generalized viscoelastic model using four parameters and differential operators of non-integer order.
- Golla-Hughes-McTavish Method (GHM) – Made by Golla, Hughes and McTavish (1986), the modulus function interpreted as being constituted by a series of mini-oscillator terms represented by three positive parameters.
- Augmenting Thermodynamic Fields (ATF) – Motivated by results from materials science, methods of irreversible thermodynamic are used to develop constitutive relations. Lesieutre and Mingori (1990) developed the method introducing a thermal coordinates in order to interact with mechanical displacement field to take into account the dissipation. Later, Lesieutre (1992) developed a one-dimensional formulation.
- Anelastic Displacement Fields (ADF) – Reported as an extension of ATF method by Lesieutre and Bianchini (1995) and Lesieutre *et al.*, 1996. In this approach, an anelastic component was introduced to take into account the energy dissipation. This component describes that part of the strain that is not instantaneously proportional to stress. The number of anelastic displacement fields will determine the dimension of the system of equations to be solved, representing the relaxation of a particular viscoelastic material.

## 2. THEORETICAL DEVELOPMENT

The constitutive equation shown in Eq. (1) can be written in time domain (Roy and Dutt, 2016). $E$, $c_i$ and $b_i$ are the ADF viscoelastic parameters; $D$ is the differential time operator $\frac{\mathrm{d}}{\mathrm{dt}}$; $p$ is the number of anelastic fields; $E(\ )$, $Num(\ )$ and $Den(\ )$ are differential time operators. $n_k$ and $m_k$ are real numbers.

$$\sigma = E\left[1-\sum_{i=1}^{p}\frac{b_i}{c_i}\frac{1}{\left[D+b_i\right]}\right]\varepsilon = \frac{\left[\sum_{k=0}^{p} n_k \frac{d^k}{dt^k}\right]}{\left[\sum_{k=0}^{p} m_k \frac{d^k}{dt^k}\right]}\varepsilon = \frac{Num(\ )}{Den(\ )}\varepsilon = E(\ )\varepsilon \tag{1}$$

When considering rotors in spin, the material internal damping effects generates forces tending to feed energy into the system, destabilizing the rotor (Cerminaro, 1999). Using the finite element technique, Özgüven and Özkan (1984) analyzes the rotor system taken into account a viscous and hysteretic nature of the material, while Roy *et al* (2008) introduce an ATF model in the rotor motion analysis. Later, Friswell *et al* (2010) extend this work. Dutt and Roy (2011) proposed a differential operator to obtain the equations of motion using Timoshenko beam elements, and later extended by Chandraker *et al.* (2013). In the same way, Roy and Dutt (2016) developed finite element model of viscoelastic composite rotor (PVC matrix reinforced by unidirectional carbon fiber).

Most importantly, on this work the analysis is intended mainly as a study of a stability boundary. Starting from constitutive equations derived from ADF method, two equations of motion are obtained and solved applying Rayleigh-Ritz approximation and Lagrangian mechanics. Conditions of instability, orbit and Shape and Directivity Index (SDI) are obtained through the solution of equations of motion.

The viscoelastic parameters are extracted from the storage modulus and loss factor (both reported in literature) and then, applying a non-linear algorithm based in optimization procedure in order to get the constitutive equations parameters.

### 2.1 Constitutive equations and application

The ADF model is applied under two distinct approaches, considering one or two anelastic fields:

- General case (tagged as model C) - A general constitutive relation, Eq. (1) using a differential modulus operator *E*( );
- Particular case (tagged as model S) - A particular constitutive relation, Eq.(3), considering the axial strain under stationary state during shaft spin.

In the first model, the differential operator *E*( ) denotes a differential modulus operator from a generalized viscoelastic model. In Eq. (1), this operator it may be seen that the differential operators *Num*( ) and *Den*( ) have polynomials of k$^{th}$ order.

In the second model, the axial stress $\sigma$ is evaluated from the general expression of shaft axial strain $\varepsilon$. The last one can be derived by trigonometric relation $\varepsilon = (r/r_0)\varepsilon_0\, cos(\phi)$, given from Fig. 1, a shaft cross section (in bend) under spin speed $\Omega$ assumed constant, and whirl speed $\omega(t)$. *dA* is the differential of cross sectional area and *r* is its distance from center, $r_0$ is the radius of cross section. *R* is the distance of cross section center from its non-bended position.

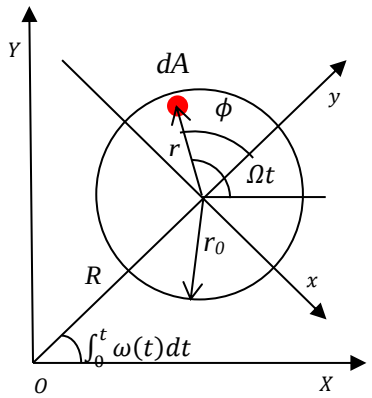


Figure 1: Cross section of a whirling shaft

Equation (3) is a development of Eq. (2) in time domain. Equation (2) is evaluated from ADF method and the expression of $\varepsilon$. The parameters *E*, $c_i$ and $b_i$ are the ADF viscoelastic parameters, $\varepsilon_0$ is the axial strain on external shaft diameter, assumed stationary during spin movement. $\Omega$ and $\omega$ are spin and whirl speeds, respectively, both assumed constant. $\dot{\phi}$ is the excitation frequency, the difference between spin and whirl speed.

$$\sigma(s) = E\left[\frac{s}{s^2+\dot{\phi}^2}\left(1-\sum_{j=1}^{p}\frac{b_i}{c_i}\left(\frac{1}{b_i+s}\right)\right)\right]\left(\frac{r}{r_0}\right)\varepsilon_0, \qquad \dot{\phi} = \Omega - \omega \tag{2}$$

$$\sigma(t) = \left[\sum_{k=0}^{p} n_k \frac{d^k}{dt^k}\right]\varepsilon(t) \tag{3}$$

In Eq. (1) and Eq. (3), $n_k$ and $m_k$ are the coefficients of constitutive equations. All of them derived from ADF viscoelastic parameters ($E$, $b_i$ and $c_i$).

For each constitutive equation, its coefficients vary according the relative viscoelastic model.

The Hysteretic model (Cerminaro, 1999) is shown in Eq. (4). Considering a rotor spin, the frequency of strain deformation is equal to the difference between rotational speed and frequency of lateral orbiting (Muszynska, 2005).

$$n_0 = E\left(\frac{1}{\sqrt{1+\eta_H{}^2}}\right) \qquad n_1 = E\left(\frac{\eta_H}{\dot{\phi}\sqrt{1+\eta_H{}^2}}\right) \tag{4}$$

The generalized ADF model with one anelastic field (referred to as 1C), is shown in Eq. (5).

$$m_0 = 1; m_1 = \frac{1}{b}; n_0 = E\left(1-\frac{1}{c}\right); n_1 = \frac{E}{b} \tag{5}$$

The generalized ADF model with two anelastic fields (referred to as 2C), is shown in Eq. (6).

$$\begin{aligned} &m_0 = 1; m_1 = \frac{1}{b_1}+\frac{1}{b_2}; m_2 = \frac{1}{b_1 b_2} \\ &n_0 = E\left(1-\left(\frac{1}{c_1}+\frac{1}{c_2}\right)\right); n_1 = E\left(\frac{1}{b_1}+\frac{1}{b_2}-\left(\frac{1}{b_1 c_2}+\frac{1}{b_2 c_1}\right)\right); n_2 = E\left(\frac{1}{b_1 b_2}\right) \end{aligned} \tag{6}$$

The particular ADF model with one anelastic field (referred to as 1S), is shown in Eq. (7)

$$n_0 = E\left[\Psi(b^2)\left[\left(1-\frac{1}{c}\right)+\left(\frac{\dot{\phi}}{b}\right)^2\right]\right]; \quad n_1 = E\left[\Psi(b)\left(\frac{1}{c}\right)\right]; \quad \Psi = \frac{1}{b^2+\dot{\phi}^2} \tag{7}$$

The particular ADF model with two anelastic fields (referred to as 2S), is shown in Eq. (8)

$$\begin{aligned} &n_0 = E\Psi_1\Psi_2\left\{\left[\left(b_1{}^2 b_2{}^2\right)\left(1-\left(\frac{1}{c_1}+\frac{1}{c_2}\right)\right)\right]+\left[\left(b_1{}^2\left(1-\frac{1}{c_1}\right)+b_2{}^2\left(1-\frac{1}{c_2}\right)\right)\right]\dot{\phi}^2+\dot{\phi}^4\right\} \\ &n_1 = E\Psi_1\Psi_2\left\{\left[\left(b_1 b_2\right)\left(\frac{b_1}{c_1}+\frac{b_2}{c_2}\right)\right]+\dot{\phi}^3\right\}; \qquad \Psi_i = \frac{1}{b_i{}^2+\dot{\phi}^2} \end{aligned} \tag{8}$$

### 2.2 Formulation and solution of equations of motion

A single rotor, Fig. 2, is considered for simulations. $L$ is length of shaft (m), $L_1$ is position of rotor (m), $h$ is thickness of disk (m), $R_2$ is radius of disk (m), $R_1$ is radius of shaft (m). An unbalance mass $m_u$ is placed on external diameter of the disk creating an unbalance $Unb$ ($kg^{-3}.m^{-3}$).

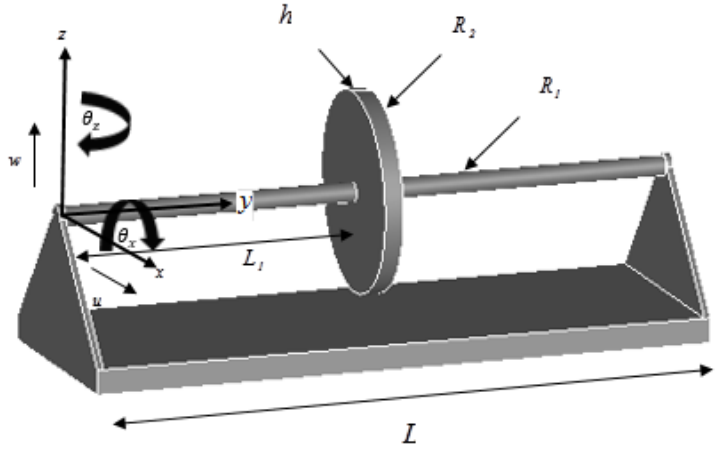


Figure 2 : Model of a simple rotor

It can be seen from Eqs. (9), (10) and (11) that the differential operator *Den( )* acts on strain generalized potential $u_T$ while *Num( )* acts on strain ε. $U_T$ is the strain generalized potential integrated over the shaft volume.

$$u_T = \int_0^{\varepsilon} \sigma d\varepsilon \qquad e \qquad U_T = \int_V u_T dV \tag{9}$$

$$[Den(\ )]u_T = \int_0^{\varepsilon} [Num(\ )](\varepsilon) d\varepsilon \tag{10}$$

$$\left[\sum_{k=0}^{p} m_k \frac{d^k}{dt^k}\right] U_T = \left[\sum_{k=0}^{p} m_k \frac{d^k}{dt^k}\right] \int_V u_T dV = \int_V \left( \int_0^{\varepsilon} \left[\sum_{k=0}^{p} n_k \frac{d^k}{dt^k}\right](\varepsilon) d\varepsilon \right) dV \tag{11}$$

According to Lallane and Ferraris (1998), adopting an approximation function $f(y) = sen(\pi y/L)$ and applying a Rayleigh-Ritz approximation, the displacements in the *x* and *z* directions, as well as rotations, can be approximated as shown in Eqs. (12), (13) and (14)

$$u(x,t) = f(y)U(t) = f(y)U; \qquad w(x,t) = f(y)W(t) = f(y)W \tag{12}$$

$$\theta_x = \frac{\partial w}{\partial y} = f'(y)W = g(y)W; \qquad \frac{\partial \theta_x}{\partial y} = f''(y)W = h(y)W \tag{13}$$

$$\theta_z = -\frac{\partial u}{\partial y} = -f''(y)U = -g(y)U; \qquad \frac{\partial \theta_z}{\partial y} = -f''(y)U = -h(y)U \tag{14}$$

Moreover, the unbalance excitation force $\{F\}$ can be derived as follows in Eq. (15) (Lallane and Ferraris, 1998)

$$\{F\} = \begin{bmatrix} m_u \Omega^2 R_2 f(L_1) sen(\Omega t) \\ m_u \Omega^2 R_2 f(L_1) cos(\Omega t) \end{bmatrix} \tag{15}$$

Using Lagrangian Mechanics and differential modulus operator *E*( ), five different models arises, each of them relative to its constitutive equation:

- Models 1C and 2C, set of Eqs. (16) and (17) - ADF, general case with one and two anelastic fields, respectively;
- Models 1S and 2S, set of Eq. (18) - ADF, particular case, with one and two anelastic fields, respectively;
- Model H, set of Eq. (18) - Equivalent internal hysteretic damping, assuming whirl speed constant.

$$\begin{cases} [M_3]\{\dddot{T}\}+[M_2]\{\ddot{T}\}+[M_1]\{\dot{T}\}+[M_0]\{T\}=\left[\sum_{k=0}^{1} m_k \frac{d^k}{dt^k}\right]\{F\} \\ [M_3]=\begin{bmatrix} m_1 s_1 & 0 \\ 0 & m_1 s_1 \end{bmatrix} \quad [M_2]=\begin{bmatrix} m_0 s_1 & -\Omega m_1 s_2 \\ \Omega m_1 s_2 & m_0 s_1 \end{bmatrix} \\ [M_1]=\begin{bmatrix} k_1 & -\Omega m_0 s_2 \\ \Omega m_0 s_2 & k_1 \end{bmatrix} \quad [M_0]=\begin{bmatrix} 2k_0 & -\Omega k_1 \\ \Omega k_1 & 2k_0 \end{bmatrix} \quad \{T\}=\begin{bmatrix} U \\ W \end{bmatrix} \end{cases} \tag{16}$$

$$\begin{cases} [M_4]\{\ddddot{T}\}+[M_3]\{\dddot{T}\}+[M_2]\{\ddot{T}\}+[M_1]\{\dot{T}\}+[M_0]\{T\}=\left[\sum_{k=0}^{2} m_k \frac{d^k}{dt^k}\right]\{F\} \\ [M_4]=\begin{bmatrix} m_2 s_1 & 0 \\ 0 & m_2 s_1 \end{bmatrix} \quad [M_3]=\begin{bmatrix} m_1 s_1 & -\Omega m_2 s_2 \\ \Omega m_2 s_2 & m_1 s_1 \end{bmatrix} \\ [M_2]=\begin{bmatrix} m_0 s_1 + k_2 & -\Omega m_1 s_2 \\ \Omega m_1 s_2 & m_0 s_1 + k_2 \end{bmatrix} \quad [M_1]=\begin{bmatrix} k_1 & -(2k_2 - m_0 s_2)\Omega \\ (2k_2 - m_0 s_2)\Omega & k_1 \end{bmatrix} \\ [M_0]=\begin{bmatrix} 2\left(k_0 - \Omega^2 k_2\right) & -k_1\Omega \\ k_1\Omega & 2\left(k_0 - \Omega^2 k_2\right) \end{bmatrix} \quad \{T\}=\begin{bmatrix} U \\ W \end{bmatrix} \end{cases} \tag{17}$$

$$\begin{cases} [M_2]\{\ddot{T}\}+[M_1]\{\dot{T}\}+[M_0]\{T\}=\{F\} \\ [M_2]=\begin{bmatrix} s_1 & 0 \\ 0 & s_1 \end{bmatrix} \quad [M_1]=\begin{bmatrix} k_1 & -\Omega s_2 \\ \Omega s_2 & k_1 \end{bmatrix} \\ [M_0]=\begin{bmatrix} 2k_0 & -k_1\Omega \\ k_1\Omega & 2k_0 \end{bmatrix} \quad \{T\}=\begin{bmatrix} U \\ W \end{bmatrix} \end{cases} \tag{18}$$

The parameters of rotor in the equation of motion follows a set of Eq. (19). $I$ is shaft area moment of inertia (m$^4$), $M_D$ is mass of disk (kg), $I_{D_x}$and $I_{D_y}$ are mass moment of inertia (kg.m$^2$) of disk in direction $x$ and $y$ respectively, $\rho$ is density of material (Kg.m$^{-3}$).

$$\begin{cases} k_0 = \frac{In_0}{2}\int_0^L h^2(y)dy \qquad k_1 = In_1\int_0^L h^2(y)dy \qquad k_2 = In_2\int_0^L h^2(y)dy \\ s_1 = M_D f^2(l_1) + I_{D_x} g^2(l_1) + \rho A\int_0^L f^2(y)dy + \rho I\int_0^L g^2(y)dy \\ s_2 = I_{D_y} g^2(l_1) + 2\rho I\int_0^L g^2(y)dy \end{cases} \tag{19}$$

All five models are represented in general form in Eq.(20), or in state-space representation, Eq. (21). The equations parameters vary according to each model considered. In Eq. (21), $\{X\}$ is the state vector and $\{Y\}$ is the vector. In time domain the equations of motion in state-space formulation are solved numerically.

$$[M_{p+2}]\frac{d^{p+2}}{dt^{p+2}}[T]+[M_{p+1}]\frac{d^{p+1}}{dt^{p+1}}[T]+\ldots[M_0][T]=\left[\sum_{k=0}^{p} m_k \frac{d^k}{dt^k}\right]\{F\} \tag{20}$$

$$\begin{cases} \begin{cases} \{\dot{X}\} = [A]\{X\} + \sum_{i=0}^{p} [B_i] \frac{d^i}{dt} \{F\} \\ \{Y\} = [C]\{X\} \end{cases} \\ \{X\} = \begin{Bmatrix} [X_1] \\ \vdots \\ \vdots \\ [X_{p+2}] \end{Bmatrix} \; ; \; [A] = \begin{bmatrix} [0] & [I] & \cdots & [0] \\ \vdots & \cdots & [I] & \vdots \\ \vdots & \cdots & \cdots & [I] \\ [A_1] & \cdots & \cdots & [A_{p+2}] \end{bmatrix} ; \; [B_i] = m_i \begin{bmatrix} [0] \\ \vdots \\ \vdots \\ [I] \end{bmatrix} \\ [A_i] = \left[ -M_{p+2}^{-1} \right] [M_i] \; ; \; [X_i] = \frac{d^{i-1}}{dt} [T] \; ; \; [T] = \begin{bmatrix} U \\ W \end{bmatrix} \; ; \; [C] = [[I] \; [0] \; \cdots \; \cdots] \end{cases} \tag{21}$$

In order to simulate a hysteretic internal equivalent damping, an aluminum rotor is used as a reference. The ADF parameters are extracted by minimizing the objective function, *B*, Eq. (22). For each ADF model, *B* is a sum of absolute error for *N* frequency responses ($H_{ADF}$) in the range from 0,01Hz to 2580Hz, considering the shaft as an Euler-Bernoulli beam under harmonic vibration in bending. A non-linear approximation algorithm finds optimal parameters minimizing all ADF transfer functions simultaneously. In Eq. (22), *B* is a transfer function for any ADF model.

For the PVC hardened rotor at 20ºC, the references are experimental results of frequency dependent loss factor ($\eta_E$) and real part of modulus ($E_E$) (Gonze and Chauffoureaux, 1973). Similarly, the ADF adjusted parameters are extracted minimizing a sum of absolute error between experimental and adjusted values for $\eta$ and *E*, considering a frequency range from 21,5Hz to 375Hz. The same approximation algorithm used for aluminum was used to find optimal ADF parameters minimizing B function for models 1C and 2C, simultaneously, as shown in Eq. (23).

For the PVC at 20ºC, the same rotor and ADF parameters from Roy and Dutt (2016) are assumed. Simulation results from Roy and Dutt (2016) are reference values in order to validate the model C of this work.

$$B = \sum_{i=1}^{N} abs \left( \frac{H_{H_i} - H_{ADF_i}}{H_{H_i}} \right) + \sum_{i=1}^{N} abs \left( \frac{Real\left(H_{H_i}\right) - Real\left(H_{ADF_i}\right)}{Real\left(H_{H_i}\right)} \right) \tag{22}$$

$$B = \sum_{i=1}^{N} abs \left( \frac{\eta_{E_i} - \eta_{A_i}}{\eta_{E_i}} \right) + abs \left( \frac{E_{E_i} - E_{A_i}}{E_{E_i}} \right) \tag{23}$$

Figure 3a plots for models “C” and “S” the adjustment values of frequency response obtained for aluminum while Fig. 3b plots the adjustment/experimental (adj/exp) values for $\eta$ and *E* considering model 2C - PVC hardened at 20ºC.

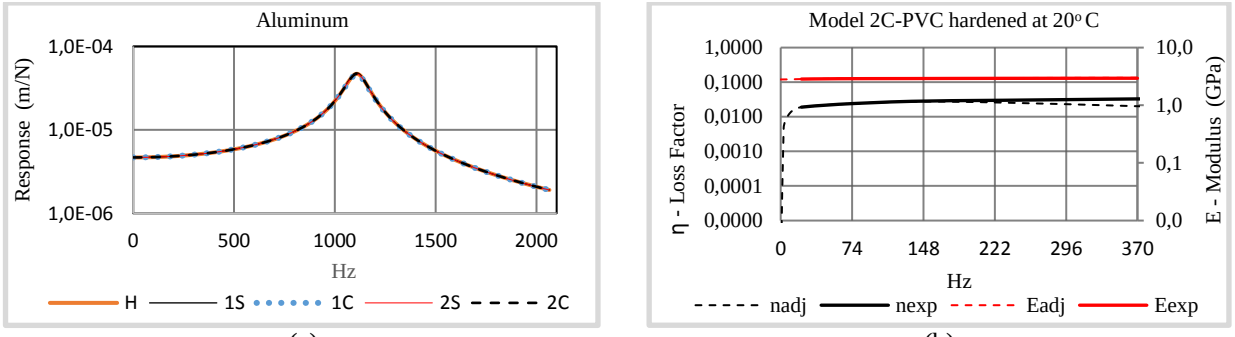


(a) (b)

Figure 3- a) Frequency response adjustments for aluminum b) Loss factor and real part of complex modulus – Adjustment for PVC hardened at 20ºC.

### 2.3 Orbit Directionality

In order to investigate the directionality of the orbit of the rotor, complex number notation can be used to represent mathematically a signal composed by two real and independent harmonic signals (Miranda, 2002). The complex signals associated with the response of a rotating system are thus defined as shown in Eq. (24)

$$P(t) = X(t) + jY(t); \qquad \overline{P}(t) = X(t) - jY(t) \tag{24}$$

where $X(t)$ and $Y(t)$ are the real signals measured orthogonally and simultaneously in a station of the rotor, and $\overline{P}(t)$ is the complex conjugate of $P(t)$. One can associate the complex signal $P(t)$ to a moving point or vector taken from the origin and whose coordinates correspond, in the complex plane, to the real and imaginary axis.

The complex signal can then be written in the polar form, through the Fourier series expansion of $X(t)$ and $Y(t)$ (Dias Jr. *et al*, 2004),

$$P(t) = P_f(t) + P_b(t) = r_f e^{j\omega t} + r_b e^{j\omega t} \tag{25}$$

so that the signal can be expressed in terms of its harmonic forward and backward components, $r_f$ and $r_b$. The direct comparison of these values defines whether the shaft whirl is forward or backward (Miranda, 2002).

- $|r_b(t)| = 0$ ➔ Circular forward precessional motion;
- $|r_f(t)| > |r_b(t)|$ ➔ Elliptical forward precessional motion;
- $|r_f(t)| = |r_b(t)|$ ➔ Rectilinear motion;
- $|r_f(t)| < |r_b(t)|$ ➔ Elliptical backward precessional motion;
- $|r_f(t)| = 0$ ➔ Circular backward precessional motion.

In order to analyze the response of a rotating machine associated to a complex signal, the concept of analytic signal must be developed. This type of signal is also complex and has the inherent characteristic of its spectrum vanished for negative frequencies. An analytic signal associated to a complex signal can be defined as being composed by the original complex signal and its Hilbert transform. Considering the complex signal, $P(t)$, and its Hilbert transform, $\hat{P}(t)$, the analytic signals of forward and backward whirl, $P_f(t)$ and $P_b(t)$, can be defined as shown in Eq. (26) (Dias Jr. *et al*, 2004),

$$P_f(t) = \left\{P(t) + j\hat{P}(t)\right\}/2; \qquad P_b(t) = \left\{P(t) - j\hat{P}(t)\right\}/2 \tag{26}$$

The corresponding Fourier transforms are:

$$P_f(\omega) = \left\{P(\omega) + (sign\omega)P(\omega)\right\}/2 = \begin{cases} P(\omega), \text{ for } \omega > 0 \\ P(\omega)/2, \text{ for } \omega = 0 \\ 0, \text{ for } \omega < 0 \end{cases};$$

$$P_b(\omega) = \left\{P(\omega) - (sign\omega)P(\omega)\right\}/2 = \begin{cases} 0, \text{ for } \omega > 0 \\ P(\omega)/2, \text{ for } \omega = 0 \\ P(\omega), \text{ for } \omega < 0 \end{cases}; \tag{27}$$

Equations (26) and (27) show that the analytic signal of forward whirl is defined for positive frequencies only, while the backward analytic signal includes only negative frequencies.

The relative amplitude between forward ($P_f$) and backward ($P_b$) components defines whether the precessional motion of a specific point of the rotor length is forward or backward, circular, elliptical or rectilinear. These two components can be combined in one parameter, called Shape and Directivity Index (SDI), Eq. (28) (Miranda, 2002).

$$-1 \le SDI = \frac{|P_f| - |P_b|}{|P_f| + |P_b|} \le 1 \tag{28}$$

The relations between the values of the SDI define the shape of a rotor station orbit and the direction of the precessional motion:

- $SDI = -1$ ➔ Circular backward precessional motion
- $-1 < SDI < 0$ ➔ Elliptical backward precessional motion
- $SDI = 0$ ➔ Rectilinear motion
- $0 < SDI < 1$ ➔ Elliptical forward precessional motion
- $SDI = 1$ ➔ Circular forward precessional motion

### 2.4 Directional Wigner distribution

There are several types of distributions that can transform a signal in time into the time-frequency plane. In this work, the Wigner distribution is used. It belongs to the so-called Cohen's class of distribution and is one of the most commonly used (Miranda, 2002). This distribution, when applied to signals that show directivity, is called directional Wigner distribution (dWD). The Wigner distribution calculated for a complex signal is defined as (Miranda, 2002)

$$dW_{pp}(t,f)=\begin{cases}\int_{-\infty}^{\infty} p_f(t+\frac{\tau}{2})\overline{p}_f(t-\frac{\tau}{2})e^{-j2\pi f}\,d\tau, & for\ f>0\\ \int_{-\infty}^{\infty} p_b(t+\frac{\tau}{2})\overline{p}_b(t-\frac{\tau}{2})e^{-j2\pi f}\,d\tau, & for\ f<0\end{cases} \tag{29}$$

In order to calculate the directional distributions, one can follow the steps bellow (Miranda, 2002):

1. Measure the real signals $X(t)$ e $Y(t)$, taken from sensors disposed perpendicularly in a station of the rotor;
2. Obtain the complex signal, as in Eq. (24);
3. Compute the Hilbert transform of the complex signal;
4. Obtain the forward and backward analytic signals, as in Eqs. (26);
5. Compute the directional Wigner distribution, as in Eq. (29).

The direct comparison of the components of $dW_{pp}(t,f)$ also defines whether the shaft whirl is forward or backward (Miranda, 2002).

## 3. RESULTS AND DISCUSSION

Rotor parameters are given on Tab. 1, for aluminum and PVC cases. The loss factor and Young Modulus for aluminum are assumed 0.02 and 7.13E10, respectively.

Table 1 – Rotor parameters

| Material | $\rho$ (Kg/m$^3$) | $L$ (m) | $L_1$ (m) | $R_1$ (m) | $R_2$ (m) | $Unb$ (kg$^{-3}$.m$^{-3}$) | $h$ (m) |
|---|---|---|---|---|---|---|---|
| Aluminum (Roy *et al*, 2016) | 2500 | 0,40 | 0,133 | 0,0100 | 0,150 | 10 | 0,030 |
| PVC (Roy and Dutt, 2016) | 1390 | 0,35 | 0,175 | 0,0175 | 0,050 | 10 | 0,020 |

Extracted viscoelastic parameters for PVC hardened are tabulated on Tab. 2.

Table 2 – ADF material parameters

| Material | Model | $b_1$ (s$^{-1}$) | $b_2$ (s$^{-1}$) | $c_1$ | $c_2$ | $E_2$ (Pa) |
|---|---|---|---|---|---|---|
| Aluminum (Roy *et al*, 2016) | 2S/2C | 217198,54 | 240710,05 | 21618,150 | 1,1027 | 7,686E+11 |
| PVC (Roy and Dutt, 2016) | 2S/2C | 159,4867 | 1,1730E+04 | 25,1428 | 1,1067 | 4,0032E+08 |
| PVC hardened at 20 ºC | 2S/2C | 178,057 | 20,427 | 20,931 | 40,932 | 3,0222E+09 |

As an example of numerical results, SLS (Stability Limit of spin Speed) for aluminum and PVC are given on Tab. 3 and (4) respectively while on Tab. 4 the models 1S and 2S are compared with 1C and 2C respectively.
For aluminum rotor, model 2S shown a good approximation when compared with hysteretic model (0,22% difference) while does not for model 2C (27,67% difference). For both models, assumed $\omega = 0.999\Omega$.
For PVC rotor, models 1C and 2C agree with the reference, validating the model with reference (0,97% and 1,65% difference), while models 1S and 2S does not agree (65,7% and 111,6 % difference). For models 1S and 2S, assumed $\omega = 0.999\Omega$.

Table 3 – Validation SLS for aluminum (RPM)

| Model | H | 2S | 2C |
|---|---|---|---|
| Ref. (Hysteretic) | 3104 | - | - |
| This work | - | 3111 | 2245 |
| % Difference | - | 0,22% | 27,67% |

Table 4 – Validation SLS for PVC at 20ºC (RPM)

| Model | 1C | 2C | 1S | 2S |
|---|---|---|---|---|
| (Roy and Dutt, 2016) | 412 | 302 | - | - |
| This work | 408 | 307 | 683 | 639 |
| % Diference | 0,97% | 1,65% | 65,7% | 111,6% |

For the model 2C in PVC hardened at 20 ºC, the orbit at spin speeds of 95% SLS, 100% SLS and 105% SLS are given on Fig. 4a, 4b and 4c, respectively. Fig 4c confirms the SLS shown in Tab. 4 where it may be seen the orbit instability.

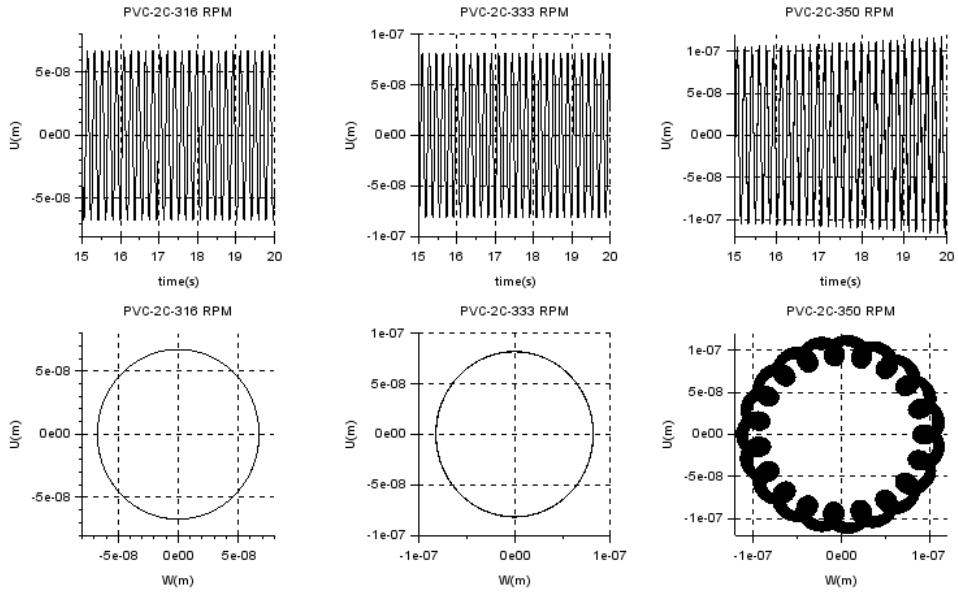


a) b) c)

Figure 4: Model 2C – PVC hardened - Orbit: a) 95% SLS, b) SLS, c) 105% SLS

For model 2S, in PVC hardened at 20 ºC, signal analysis in time-frequency domain are given in Fig. 5. SDI is always greater than zero, but not equal to 1. This indicates that the rotor does not experience a backward whirl, but a SDI value different from unit suggests that a backward component is present, confirmed by negative part of directional Wigner distribution of Fig. 5. Once the rotor under study is isotropically supported, the nature of backward component can be associated to the nature of viscoelasticity.

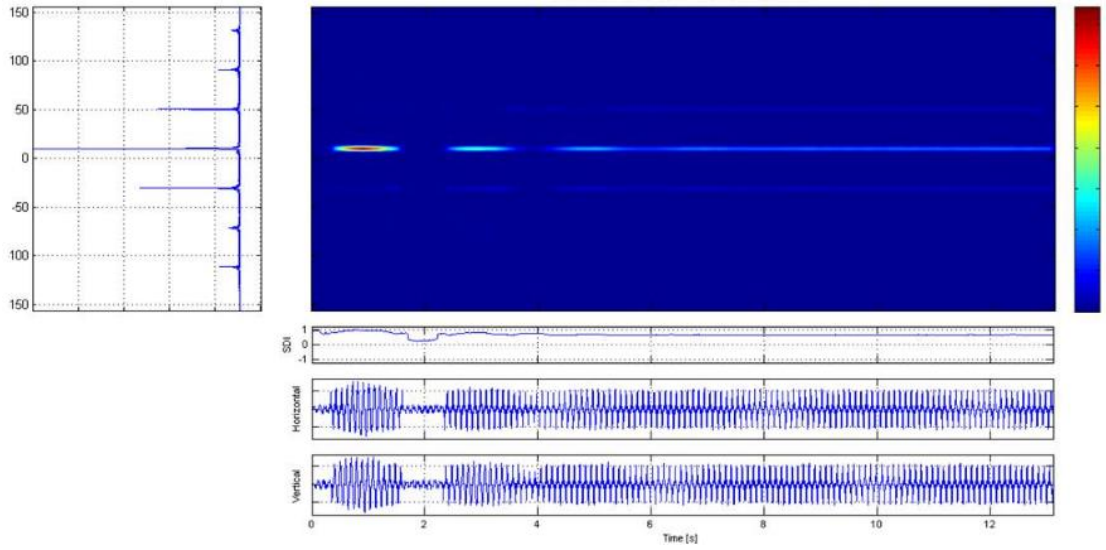


Figure 5: Time-frequency response when spin speed is 5% smaller than SLS - PVC hardened at 20 ºC - 2S model

## 4. CONCLUSION

The models 1C and 2C obtained a good approximation when comparing SLS speeds with the results of Roy and Dutt (2016).

A good approximation for SLS speed was given for the models 1S and 2S for aluminum rotors.

Considering the model 2S in PVC, there are components in retrograde precession, although to a lesser extent than as direct precession.

Studies regarding directivity of the rotor should be more investigated, especially with experimental results.

## 5. REFERENCES

Bagley, R.L., and Torvik, P.J., 1983. "Fractional calculus - A different approach to the analysis of viscoelastically damped structures". *AIAA Journal*, Vol. 21, No. 5, pp. 741-748.

Cerminaro, A.M., 1999. *Simulation of Internal Damping in a Rotating System Supported by Magnetic Bearings*. Master of Science Thesis, TUFTS UNIVERSITY, Medford.

Chandraker, S., Roy, H. and Maurya, G., 2013. "Modal Analysis of Multi Layer Viscoelastic Rotors Considering Higher Order Model". In *Proceedings of the ASME 2013 Gas Turbine India Conference*. Bangalore, Karnataka, India.

Dias Jr, M., Miranda, U.A., Idehara, S.J. and Mesquita, A.L.A., 2004. "On the application of directional time-frequency distributions to the identification of simultaneous forward and backward whirling in flexible rotors". *Australian Journal of Mechanical Engineering*, Vol. 1, No. 2, p. 103-112.

Dutt, J.K., and Roy, H., 2011. "Viscoelastic modelling of rotor-shaft systems using an operator-based approach". *Proceedings of the Institution of Mechanical Engineers, Part C: Journal of Mechanical Engineering Science*, Vol. 225, No. 1, p. 73-87.

Friswell, M.I., Dutt, J.K., Adhikari, S. and Lees, A.W., 2010. "Time domain analysis of a viscoelastic rotor using internal variable models". *International Journal of Mechanical Sciences*, Vol 52, No.10, p. 1319-1324.

Golla, D.F., 1986. *Dynamics of viscoelastic structures: a time-domain finite element formulation*. Dissertation, University of Toronto.

Gonze, A. and Chauffoureaux, J.C., 1973. "A collaborative study of the dynamic mechanical and impact properties of PVC". *Pure and Applied Chemistry*, Vol. 35, No. 3, p. 315-352.

Lalanne, M., and Ferraris, G., 1998. *Rotordynamics Prediction in Engineering*. John Wiley & Sons.

Lesieutre, G.A. 1992. "Finite elements for dynamic modelling of uniaxial rods with frequency-dependent material properties", *International. Journal of Solids and Structures*, Vol. 29, No. 12, p. 1567-1579.

Lesieutre, G.A. and Mingori, D.L., 1990. "Direct time-domain, finite element modeling of frequency-dependent material damping using augmenting thermodynamic fields (ATF)". In *Proceedings of the 30th Structures, Structural Dynamics and Materials Conference*, Mobile,AL,U.S.A.

Lesieutre, G.A., Bianchini, E. "Time domain modeling of linear viscoelasticity using anelastic displacement fields." *Journal of vibration and acoustics* 117.4 (1995): 424-430.

Lesieutre, G.A.,Bianchini,E., and Maiani, A.. "Finite element modeling of one-dimensional viscoelastic structures using anelastic displacement fields." *Journal of Guidance, Control, and Dynamics* 19.3 (1996): 520-527.

Miranda, U.A., 2002. *Aplicação de métodos de análise tempo-frequência ao estudo de sistemas rotativos*. Master of Science Thesis, UNICAMP, Campinas.

Muszynska, A., 2005. *Rotordynamics*. CRC Press.

Özgüven, H.N., and Özkan, Z.L., 1984. "Whirl speeds and unbalance response of multibearing rotors using finite elements". *Journal of Vibration, Acoustics, Stress and Reliability in Design*, Vol. 106, No. 1, p. 72-79.

Roy, H. and Dutt, J.K, 2016. "Dynamics of polymer and polymer composite rotors–An operator based finite element approach". *Applied Mathematical Modelling*, Vol. 40, No. 3, p. 1754-1768.

Roy, H., Dutt, J.K. and Datta, P.K., 2008. "Dynamics of a viscoelastic rotor shaft using augmenting thermodynamic fields - a finite element approach". *International Journal of Mechanical Sciences*, Vol 50, No.4, p. 845-853.

Roy, H., Chandraker, S., Dutt, J.K. and Roy, T., 2016. "Dynamics of multilayer, multidisc viscoelastic rotor–An operator based higher order classical model". *Journal of Sound and Vibration*, Vol. 369, p. 87-108.

## 6. RESPONSIBILITY NOTICE

The authors are the only responsible for the printed material included in this paper.